# Piloted Simulation of an Onboard Trajectory Optimization Algorithm

Douglas B. Price*
*NASA Langley Research Center, Hampton, Virginia*
and
Anthony J. Calise† and Daniel D. Moerder‡
*Drexel University, Philadelphia, Pennsylvania*

**This paper describes a real-time piloted simulation of algorithms designed for onboard computation of time-optimal intercept trajectories for an F-8 aircraft. The algorithms, derived using singular perturbation theory, generate commands that are displayed to the pilot using the flight director needles of the 8-ball. By zeroing out the horizontal and vertical needles, the pilot flies an approximation to a time-optimal intercept trajectory. The available display and computation modes are described and the results are presented illustrating the performance of the algorithms with a pilot in the loop.**

## Nomenclature

$C_D$ = drag coefficient
$C_{D_0}$ = drag coefficient for $\alpha = 0$
$C_L$ = lift coefficient
$C_{L_\alpha}$ = slope of lift coefficient curve, 1/rad
$D$ = drag, N
$D_0$ = drag for $L = W$, N
$E$ = total energy per unit weight, m
$E_0$ = long-range cruise energy level, m
$G$ = load factor
$H$ = variational Hamiltonian
$h$ = altitude, m
$K$ = induced drag parameter
$K_1, K_2$ = gains, 1/s
$L$ = lift, N
$L_n$ = horizontal lift component, N
$L_\gamma$ = vertical lift component, N
$M$ = Mach number
$m$ = mass, kg
$q$ = dynamic pressure, N/m$^2$
$R$ = range, m
$S$ = reference area, m$^2$
$T$ = thrust, N
$t$ = time
$V$ = velocity, m/s
$W$ = weight, N
$x,y$ = target centered horizontal axes, m
$\alpha$ = angle of attack, rad
$\beta$ = heading, rad
$\gamma$ = flight-path angle, rad
$\delta(\ )$ = perturbation associated with a particular variable
$\epsilon$ = small parameter used for singular perturbation analysis
$\eta$ = induced drag parameter
$\lambda$ = line-of-sight angle, rad
$\gamma_d$ = desired flight-path angle, rad
$\lambda_E$ = energy costate, s/m
$\lambda_x, \lambda_y$ = position costates, s/m
$\lambda_\beta$ = heading costate, s/rad
$\mu$ = bank angle, rad
$\rho$ = air density, kg/m$^3$

*Subscripts*

$C$ = climb
$D$ = descent
$f$ = final
max = maximum
min = minimum
$T$ = target
$0$ = outer solution variable or solution
$1,2$ = boundary-layer variables or solution

*Superscripts*

$c$ = climb
$d$ = descent

## Introduction

THIS study was initiated to test and demonstrate the feasibility of computing optimal trajectories onboard an aircraft in real time. The computation of optimal trajectories is a complex numerical problem which has required computers that cannot be flown aboard an airplane. The state-of-the-art in small, powerful computers recently has improved enough so that a solution of this problems is now feasible. Even with modern computers, the complexity of the problem of computing optimal trajectories requires simplifications and the use of efficient algorithms to accomplish the task. Recent work on the application of singular perturbation techniques to trajectory optimization problems has been used here to develop the needed algorithms.[1,2]

Applications of singular perturbation theory to flight mechanics problems have, to date, centered primarily on aircraft trajectory optimization. In the late sixties and early seventies, a number of papers appeared in which energy state and other reduced-order modeling methods were introduced.[3,4] Matched asymptotic expansions were employed somewhat later.[5,6] The long-range, three-dimensional minimum-time intercept problem also has been studied.[7] The deri-

Submitted July 2, 1982; revision received June 22, 1983. This paper is declared a work of the U.S. Government and therefore is in the public domain.

*Aero-Space Technologist, Flight Dynamics and Control Division, Theoretical Mechanics Branch.
†Professor, Department of Mechanical Engineering and Mechanics.
‡Research Assistant, Department of Mechanical Engineering and Mechanics.

vation of the results presented in this paper is based mainly on a multi-time-scale method.[6]

The particular problem of time optimal intercept trajectories for aircraft was chosen as a representative task for onboard trajectory computation for several reasons. This problem occurs in a number of real situations that range from computation of minimum time trajectories to a fixed point to air combat scenarios. Also, the singular perturbation formulation of this problem allows for a good bit of off-line computation which serves to minimize the amount of computation that must be done in real time. These aspects will be discussed in more detail in a later section.

This work should be considered as demonstration of a trajectory optimization algorithm which has been mechanized in real time and with a realistic aircraft simulation. The techniques applied here to generate algorithms for the time-optimal intercept problem can be applied to other optimization problems as well. Also, the concept of relying on the pilot for implementation of the commands displayed to him rather than executing them automatically is useful for many situations where a very sophisticated automatic control system would be undesirable.

## Description of Simulation

The F-8 aircraft was chosen for this simulation because of the availability of a very realistic simulation of NASA's Digital Fly-by-Wire (DFBW) aircraft, which is an F-8C modified so that the only link between the pilot and the aerodynamic control surfaces is through the onboard digital computer. The flight envelope of the DFBW aircraft is shown in Fig. 1. The zero energy rate contour defines the limits of level steady-state flight with full thrust and afterburner. This contour along with the dynamic pressure limit below 5100 m altitude and the maximum angle-of-attack boundary at low speed define the envelope for steady-state flight.

The Langley simulation of the DFBW aircraft uses a complete six-degree-of-freedom model that accurately represents the aircraft throughout its flight envelope. This software is resident on Langley's Real Time Digital Simulation System consisting of several CDC 6000 series and Cyber 175 computers and associated analog and digital interfaces.

The cockpit used for the simulation is a general-purpose fixed-base cockpit used at LaRC to represent various types of aircraft from small general aviation airplanes to the Space Shuttle. For the F-8 simulation, this cockpit has the standard instrumentation necessary for determining aircraft attitude, velocity, acceleration, angle of attack, and sideslip angle. The rudder pedals are standard for a jet fighter, the throttle is from an actual F-8 cockpit, and the stick is a sidearm stick with force rather than displacement transducers.

The information generated by the optimal trajectory algorithms is presented to the pilot by flight director needles on the attitude indicator at the center of the instrumentation panel. His task is to keep both horizontal and vertical needles centered in order to remain on the optimal intercept trajectory. In addition, the pilot modulates the throttle during the descent part of the trajectory to null a display indicating desired thrust.

## Problem Formulation

The point mass equations of motion for the aircraft are referenced to a horizontal, target centered, inertial coordinate frame:

$$\dot{x} = V\cos\gamma\cos\beta \tag{1}$$

$$\dot{y} = V\cos\gamma\sin\beta - V_T\cos\gamma_T \tag{2}$$

$$\dot{E} = (T-D)V/W \tag{3}$$

$$\dot{\beta} = L\sin\mu/(mV\cos\gamma) \tag{4}$$

$$\dot{h} = V\sin\gamma \tag{5}$$

$$\dot{\gamma} = (L\cos\mu - W\cos\gamma)/mV \tag{6}$$

The variables in Eqs. (1-6) are defined with the aid of Fig. 2 where the subscript $T$ is used to designate the target. For the purpose of generating control algorithms, it is assumed that the target is flying with constant velocity $V_T$, not necessarily in a horizontal plane. The point mass equations are valid for a flat Earth, with thrust $T$ directed along the flight path, and weight constant. Drag $D$ is assumed to have conventional parabolic form

$$D = qSC_{D_0} + KL^2/(qS) \tag{7}$$

$$q = \rho V^2/2 \tag{8}$$

where $q$ is the dynamic pressure, $\rho$ is the air density, and

$$K = \eta/C_{L_\alpha} \tag{9}$$

$$L = qSC_L = qS(C_{L_\alpha}\alpha) \tag{10}$$

The variable $E$ is the total aircraft energy (kinetic plus potential) per unit weight

$$E = h + V^2/(2g) \tag{11}$$

where $h$ is the aircraft altitude. The control variables are aircraft lift $L$, bank angle $\mu$, and thrust $T$. The objective is to

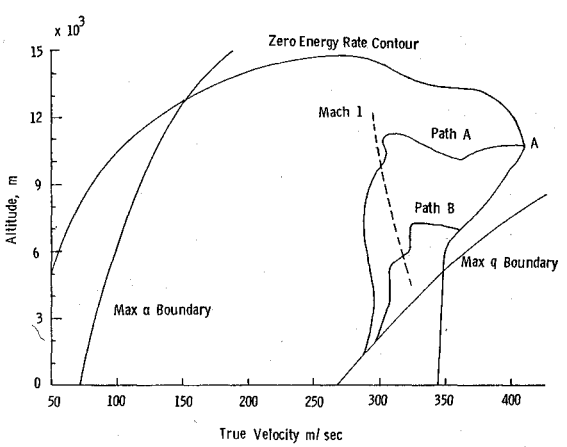


**Fig. 1 Flight envelope for F-8.**

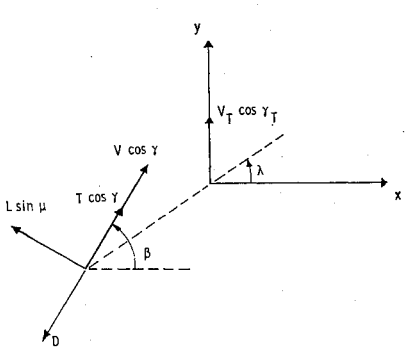


**Fig. 2 Horizontal projection of intercept geometry.**

find the controls $L$, $d$, $T$ that minimize

$$J=\int_0^{t_f} dt \tag{12}$$

subject to the following state and control variable constraints:

$$L \le WG_{\max} \tag{13}$$

$$L \le qSC_{L_\alpha}\alpha_{\max} \tag{14}$$

$$T_{\min}(h,M) \le T \le T_{\max}(h,M) \tag{15}$$

$$q \le q_{\max}, \qquad M \le M_{\max}(h) \tag{16}$$

where $G_{\max}$ is the maximum load factor, $\alpha_{\max}$ the stall angle of attack, $T_{\min}$ and $T_{\max}$ the thrust level limits that are functions of aircraft altitude and Mach $M$. The boundary conditions are such that the initial aircraft state is fully specified and require

$$x(t_f)=y(t_f)=0,\ h(t_f)=h_T(t_f) \tag{17}$$

for intercept, where $h_T(t_f)$ is taken as the projected target motion in altitude

$$h_T(t_f)=h_T(0)+(V_T\sin\gamma_T)t_f \tag{18}$$

## Summary of Control Algorithm

A total of two control modes and four display modes have been implemented. Any display and control mode combination may be selected by the pilot to drive the flight director needles. The display modes are: 1) lift and bank angle command; 2) altitude rate and heading command; 3) Mach and heading command; and 4) cruise altitude and heading command. The control modes are designated as control modes I and II. The algorithms that are used to compute the display variables for both control modes are described below.

### Control Modes I and II

The control mode I algorithm is based on a singular perturbation solution to the three-dimensional minimum time intercept problem, in which horizontal velocity, energy rate, and heading rate dynamics have been optimized on separate time scales.[2] This is done analytically by multiplying the left-hand side of Eqs. (3-6) by increasing powers of $\epsilon$ and expanding the solution to these equations as a power series in $\epsilon$. The power series approximations are substituted into Eqs. (1-6) and coefficients of corresponding terms equated to arrive at a new set of equations. This technique is useful only if the power series expansions are truncated at low order, and for this study zeroth-order expansions are used. The four boundary layers are separated by rescaling time as $\tau_i=t/\epsilon^i, i=1,\ldots,4$, respectively, then setting $\epsilon=0$ in the resulting equations. The control algorithm is summarized by the following set of equations.

Outer solution (optimal cruise):

$$h_0,E_0=\arg\{\max_{h,E}(V)\} \tag{19}$$

$$\beta_0=\sin^{-1}\{V_T\cos\gamma_T\cos\lambda/V_0\}+\lambda \tag{20}$$

$$\lambda_{x_0}=-\cos\beta_0/(V_0-V_T\cos\gamma_T\sin\beta_0) \tag{21}$$

$$\lambda_{y_0}=-\sin\beta_0/(V_0-V_T\cos\gamma_T\sin\beta_0) \tag{22}$$

$$V_0=\sqrt{(E_0-h_0)2g} \tag{23}$$

First boundary layer (optimal climb and descent):

$$h_1^c=\arg\min_h\left\{\frac{(T_{\max}-D_0)V}{V-V_0}\right\}E=E_{\text{current}} \quad T_{\max}>D \tag{24}$$

$$h_1^d=\arg\max_h\left\{\frac{(T_{\min}-D_0)V}{V-V_0}\right\}E=E_{\text{current}} \quad T_{\min}<D \tag{25}$$

$$\lambda_{E_1}=-WH_0(E,h_1)/[V_1(T_1-D_0)] \tag{26}$$

where $V_1$ and $h_1$ are the conditions along the climb (descent) path, and

$$H_0=\lambda_{x_0}V_1\cos\beta_0+\lambda_{y_0}(V_1\sin\beta_0-V_T\cos\gamma_T)+1 \tag{27}$$

$$T_1=T_{\max}\text{ for climb or }T_{\min}\text{ for descent} \tag{28}$$

$$D_0=qSC_{D_0}+KW^2/(qS) \tag{29}$$

Second boundary layer (optimal turn):

$$L_{n_2}=\sqrt{-qsWH_1(E,h,\beta)/(VK\lambda_{E_1})}*\text{sign}(\beta_0-\beta) \tag{30}$$

$$h_2=\arg\left\{(\min_{h_1}[-\rho/(H_1(E,h,\beta)KV)]\right\}$$

$$E=E_{\text{current}},\ \beta=\beta_{\text{current}} \tag{31}$$

$$\lambda_{\beta_2}=-2H_1(E,h_2,\beta)mV_2/L_{n_2} \tag{32}$$

where $V_2$ is the velocity corresponding to $E$ and $h_2$, and

$$H_1=H_0+\lambda_E(T-D_0)V/W \tag{33}$$

where $H_1=H_0(E,h,\beta)$. The geometric variables used in the above equations are defined in Fig. 2. All of the solutions are subject to the aerodynamic and propulsion limits given by Eqs. (13-16). Equation (19) in the outer solution provides the optimal (maximum velocity) cruise condition for long-range intercepts, which is shown as point A in Fig. 1. This can be computed off line since it is independent of target parameters $(V_T,\gamma_T,\lambda_T)$. The intercept heading $\beta_0$ and outer solution costates $(\lambda_{x_0},\lambda_{y_0})$ must be computed on line. The first boundary-layer solution gives the optimal climb and descent paths $(h_1^c,h_1^d)$ as a function of current total energy. These functions can also be precomputed and stored. The energy costate $(\lambda_{E_1})$ must be computed on line. The second boundary layer computes the horizontal lift component needed to null the heading error $(\beta_0-\beta)$, and the desired altitude for turning. The computation of $L_{n_2},h_2$, and $\lambda_{\beta_2}$ must be performed on line. Due to the asymptotic nature of the solution, the following limits hold[2]:

$$\lim_{\beta\to\beta_0}h_2=h_1,\quad \lim_{\beta\to\beta_0}L_{n_2}=0 \tag{34}$$

$$\lim_{\beta\to E_0}h_1=h_0 \tag{35}$$

These conditions are easily verified by using the conditions that $H_1(E,h_1,\beta_0)=0$ and $H_0(h_0,E_0)=0$, which follow since we are dealing with a free time problem.

In control mode I, $h$ and $\gamma$ dynamics are not optimized, and the vertical lift component is derived using the following proportional control law to follow $h_2$:

$$\gamma_d=K_1(h_2-h)/V+\dot{E}\frac{dh_1}{dE}\Big/V \tag{36}$$

$$L_\gamma=K_2mV(\gamma_d-\gamma)+W\cos\gamma \tag{37}$$

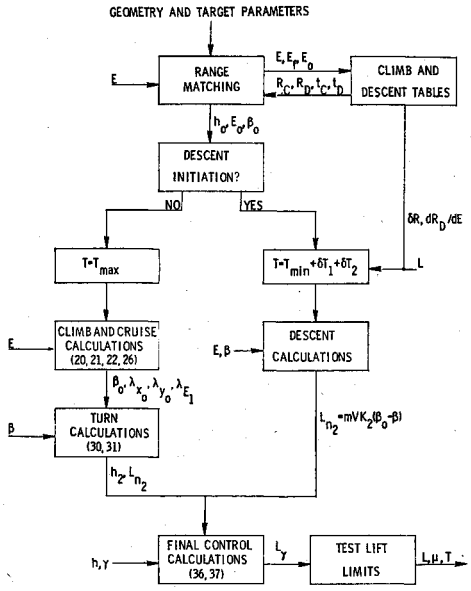


**Fig. 3 Summary of control calculations for control mode I.**

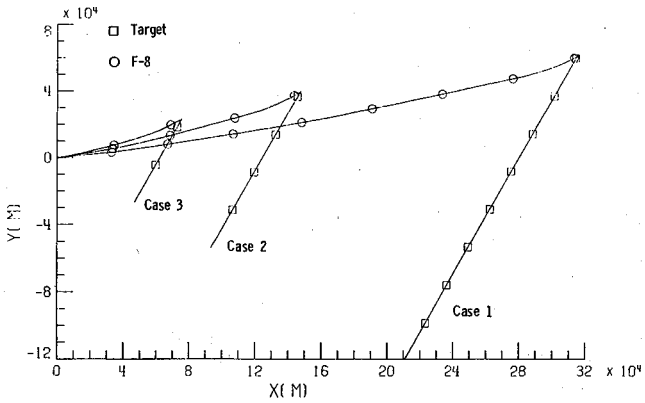


**Fig. 4 Ground tracks for cases 1-3.**

The second term in Eq. (36) accounts for the nonzero $\gamma$ needed to follow the climb and descent paths. The constants $K_1$ and $K_2$ are chosen to yield reasonable response without excessive lift. Control mode II accounts for $h$ and $\gamma$ dynamics during climb, by computing appropriate third and fourth boundary-layer solutions.[2] In order to be brief, the expressions for these solutions are omitted.

Control mode I is always used during descent since the optimal control solution calls for bang-bang lift control. This property of the solution is due to the fact that minimum time control calls for descent at minimum energy rate. Thus, even in the absence of altitude or heading error, a chattering in lift occurs in the ideal case, although this is undesirable from a piloting point of view.

*Range Matching*

The long-range optimal climb path for the F-8 is labeled as path A in Fig. 1. The optimum descent path is along the dynamic pressure boundary. Long-range intercepts are made up of climb, cruise, and descent legs. Descent initiation is accomplished by comparing the current estimated horizontal range to intercept with precomputed and stored values of horizontal range flown along the descent path.

Short-range trajectories follow optimal climb paths to "pseudocruise" energy levels which are lower than the optimal long-range cruise energy and are generated by constraining $E_0$ in Eq. (19).[8] A family of climb paths are generated and stored for a range of values for $E_0$. A typical short-range climb path is labeled as path B in Fig. 1. For short-range intercepts, $E_0$ must be found such that the horizontal climb range from $E$ to $E_0$ plus the descent range from $E_0$ to $E_f$ equals the predicted range of intercept. The final energy is chosen such that

$$h_1^q(E_f) = h_T \tag{38}$$

The procedure is slightly more complicated for nonzero $\gamma_T$. A detailed explanation of the range matching procedure can be found in Ref. 1.

*Thrust Control During Descent*

Thrust modulation is used to control descent rate so that the range matching condition is satisfied. Two correction terms are introduced.

$$T = T_{\min} + \delta T_1 + \delta T_2 \tag{39}$$

The first term corrects for the fact that $L$ does not equal $W$ during descent.

$$\delta T_1 = K(L^2 - W^3)/(qs) \tag{40}$$

The second term compensates for the current mismatch ($\delta R$) in horizontal range.

$$\delta T_2 = W\delta R/V\cos(\beta^0 - \lambda)\frac{dR_D}{dE} \tag{41}$$

*where* $R_D$ is the horizontal descent range from $E$ to $E_f$ along the descent path. The reader is again referred to Ref. 1 for details. In order to allow for both positive and negative throttling, $T_{\min}$ is nominally selected as midway between idle power and military thrust. For climb, $T_{\max}$ is chosen as maximum thrust with afterburner. A block diagram for the mode I conrol algorithm is given in Fig. 3.

*Display Modes*

As discussed earlier, the pilot may choose any one of four modes for driving the flight director needles in the cockpit display. The lift and bank angle display mode uses $L_\gamma$ and $L_{n_2}$ from Eqs. (30) and (37) for the control mode I, or from the third and fourth boundary-layer solutions in Ref. 2 for control mode II. The altitude rate and heading command mode uses Eqs. (20) and (36) in control mode I, and the third boundary-layer solution for $\gamma_d$ from Ref. 2 in place of Eq. (36) during climb for control mode II. The Mach and heading command mode is based on Eqs. (20), (24), and (25) for both control modes. The cruise Mach and heading mode is a pilot director mode which uses only the outer solution Eqs. (19) and (20). No descent guidance is given to the pilot in this mode.

These four display modes were chosen both to allow the pilot a choice in the amount of direction he wants to see and also to have a choice as to the degree of complexity of the algorithms used to drive the flight director needles. The lift and bank angle display may be considered as a direct stick command, since the flight director needles respond immediately to inputs from the control stick. This mode also requires the most computation for implementation. The altitude rate and heading command mode allows the pilot more of a choice in how he flies the airplane and requires less computation than the previous mode. Similarly, the Mach number command requires less of the computer and more of the pilot than the altitude rate.

## Numerical Results

The state and control variable constraints enforced for this problem are defined by:

$$G_{\max} = 6.5, \quad \alpha_{\max} = 20 \text{ deg}$$

$$q_{\max} = 43{,}092 \text{ N/m}^2, \quad M_{\max} = 1.6$$

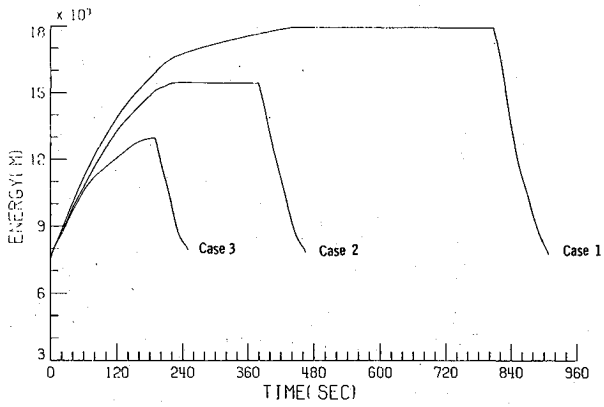


Fig. 5 Energy vs time for cases 1-3.

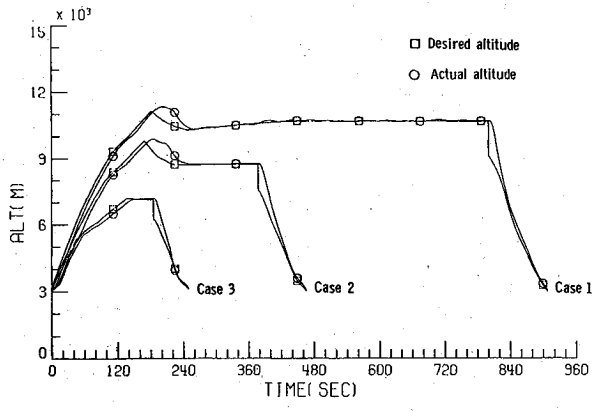


Fig. 6 Altitude vs time for cases 1-3.

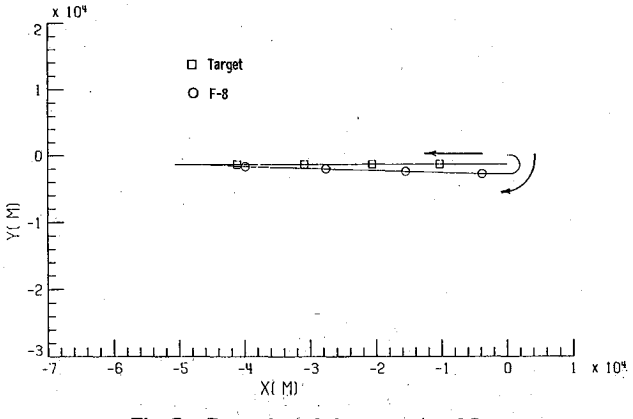


Fig. 7 Ground track for cases 4 and 5.

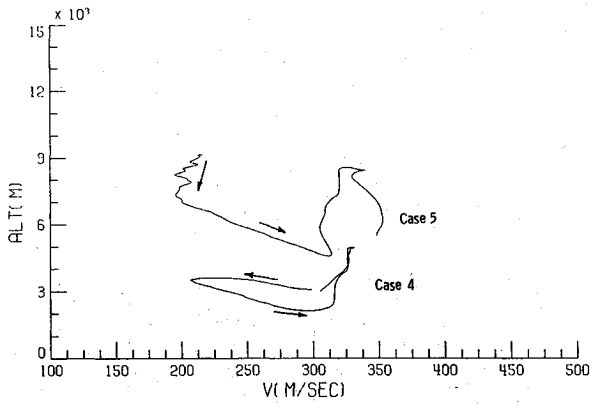


Fig. 8 Altitude vs velocity for cases 4 and 5.

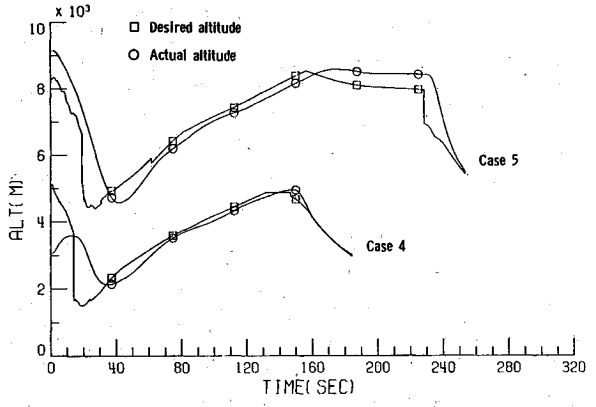


Fig. 9 Altitude vs time for cases 4 and 5.

The miniumum and maximum thrust are functions of altitude and Mach number, and their definitions have been given in the previous section.

The first five cases shown all were flown using control mode II and display mode 1 which shows the pilot desired lift/weight and desired bank angle. The last two cases will compare control modes I and II, and are different display mode. Figure 4 shows horizontal projections of the intercept geometry for several cases. Cases 1-3 are intercepts with the same geometry but different initial ranges. In each of these cases, the target is moving in a horizontal plane with a constant velocity of 232.6 m/s. The F-8 is initially heading along the positive $x$ axis. The initial range to the target for each of these three cases is different to show the effect of range matching calculation in picking different pseudocruise energies. This can be seen in Fig. 5 which shows energy vs time for cases 1-3. Case 1 is a long-range intercept in that there is a part of the trajectory flown at approximately the optimum cruise energy for the F-8. Cases 2 and 3 are short-range intercepts in that the pilot is commanded to fly to lower pseudocruise energy levels, prior to descent initiation. If a continuum of possible pseudocruise energies was allowed, instead of a discrete set, then the short-range trajectories would consist of a climb to the pseudocruise energy, followed by an immediate descent to the target. The discretization results in trajectories (such as case 2) where the F-8 flies at the pseudocruise energy level for a short period of time.

Figure 6 shows altitude and commanded altitude vs time for cases 1-3. This demonstrates the different altitudes corresponding to the pseudocruise energies shown in Fig. 5. The apparent lag in altitude along the climb path is a result of using a zeroth-order singular perturbation solution, which fundamentally behaves like a type 1 controller. That is, the commanded altitude is assumed constant in the third and fourth boundary-layer solution for vertical lift, whereas desired altitude [Eq. (24)] actually behaves more like a ramp due to the positive energy rate. Note the overshoot that results near the top of the climb where the desired altitude decreases with increasing energy. The descent part of the trajectory is flown using control mode I which has a correction for nonzero flight-path angle and, therefore, has negligible steady-state error in altitude. The corner at the top of the desired altitude trajectory and the vertical drop at the start of descent are indications that the descent path is computed using incomplete dynamics and cannot be flown exactly.

Figure 7 shows the ground track corresponding to cases 4 and 5 that require a large initial maneuver. For both cases, the F-8 starts adjacent to the target but heading in the opposite direction which necessitates an immediate high-$G$ 180 deg turn.

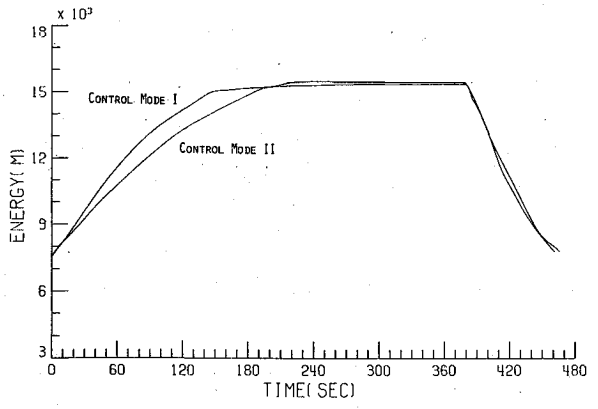


**Fig. 10 Energy vs time for control modes I and II.**

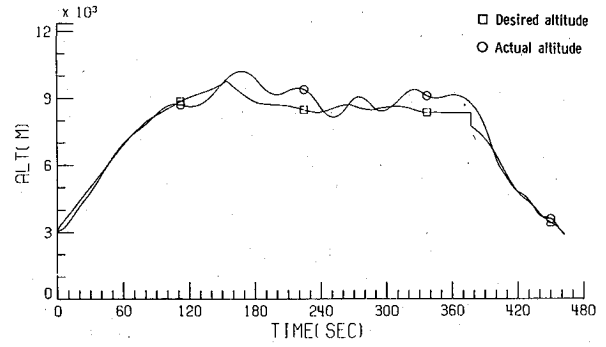


**Fig. 11 Altitude vs time with display mode 3.**

Figure 8 shows altitude vs velocity for cases 4 and 5. For cases 4 the F-8 and target are both at 3048 m altitude and the F-8's velocity is above the corner velocity (the velocity for maximum turn rate) for that altitude of about 196 m/s. Therefore, the algorithm directs the pilot to pull up initially to reduce the velocity in addition to making the 180 deg turn. This is called a high-speed yo-yo maneuver. By the time the turn is completed, the F-8 is at about 300 m/s and begins the climb to a very short pseudocruise leg before descending to the target.

Case 5 illustrates the opposite maneuver in that the F-8 starts at 9144 m altitude and at a velocity lower than the corner velocity at that altitude of about 252 m/s. The F-8, therefore, dives to gain velocity while making the 180 deg turn. This maneuver is sometimes called a low-speed yo-yo. Figure 9 shows actual and commanded altitude vs time for cases 4 and 5. The traces for case 4 illustrate the initial climb to achieve corner velocity and the immediate dive to the climb path. For case 5, the altitude descrepancy at the top of the trajectory is an indication that the F-8 is lagging behind the desired altitude and the altitude error would decrease if not cut short by the initiation of descent.

Each of the trajectories shown so far was flown using display mode 1 and control mode II. Control mode 1 does not optimize altitude and flight-path angle dynamics; however, it has a term which corrects for nonzero flight-path angle on the climb path. For this reason, the commands generated in control mode I allow the F-8 to follow the desired climb path better than control mode II. The effect of this can be seen in Fig. 10 which compares energy vs time for case 2 for control modes I and II. In control mode I, the pilot is directed to climb at a steeper angle thereby gaining energy faster. A first order (in $\epsilon$) expansion for flight path angle dynamics would have the effect of increasing the energy rate in climb for mode II, but at a considerable computational cost.

Display modes 2 and 3 which show the pilot desired altitude rate and desired Mach number, respectively, on the horizontal needle and desired heading on the vertical needle were also flown for case 2 as a comparison with display mode 1. These displays are more difficult for the pilot to fly since he must anticipate the motion of the horizontal needle to a greater degree than in display mode 1. While the altitude rate display is not too hard to follow and is mainly just a matter of learning to lead the needle, the display of desired Mach number is very difficult to follow. Figure 11 shows the desired and actual altitude for case 2 flown with display mode 3. The phugoid-like oscillations in the cruise segment of the flight occur because of the lag in the response of Mach number to pilot inputs and are difficult to eliminate. In spite of this difficulty, it was found that the pilots could easily intercept the target using information generated by any of the three display modes discussed here. Miss distances to the target were typically less than 100 m.

Since we did not use a separate computer system to perform the onboard calculations, they were done by the CDC Cyber 175 system along with all calculations required to run the simulation. In order to obtain an estimate of the time required to perform the onboard calculations, a timing routine was used under a number of different flight conditions with the display and control modes that require the most computations. The average time required to go through the onboard algorithms for all of these conditions was 0.0012 s, with a maximum time of 0.0015 s and a minimum of 0.0011 s. The memory required for the algorithms on the CDC computer was 47,744 octal 60 bit words. The number of words required for the programs themselves was 6773 octal with the rest going to storage (common blocks). No attempt was made to optimize the program from the point of view of either time or memory requirements.

## Conclusions

This study demonstrates a trajectory optimization algorithm which has been mechanized in real time with a complete and realistic simulation of an aircraft. The problem chosen to demonstrate the technique here was time-optimal intercept for an F-8 aircraft. The pilot flew the simulated aircraft using various display options to tell him how to fly in a time-optimal manner. It was shown that a pilot can use the displays to intercept a constant velocity target effectively. The intercept trajectories generated in this manner follow realistic three-dimensional paths including vertical plane maneuvers. Even though the algorithms were derived under the assumption of constant target velocity, the feedback form of the control solution makes it adaptive to changes in target motion parameters. The ability to adapt to maneuvering targets is limited only by the speed of the onboard computer.

## References

[1] Calise, A. J., "Singular Perturbation Techniques for On-Line Optimal Flight Path Control," *Journal of Guidance and Control*, Vol. 4, July-Aug. 1981, pp. 398-405.

[2] Calise, A. J. and Moerder, D. D., "Singular Perturbation Techniques for Real Time Aircraft Trajectory Optimization and Control," NASA CR-3597, 1982.

[3] Bryson, A. E. Jr., Desai, M. N., and Hoffman, W. C., "Energy State Approximation in Performance Optimization of Supersonic Aircraft," *Journal of Aircraft*, Vol. 6, Nov.-Dec. 1969, pp. 481-488.

[4] Kelley, H. J., and Edelbaum, T. N., "Energy Climbs, Energy Turns and Asymptotic Expansions," *Journal of Aircraft*, Vol. 7, Jan.-Feb. 1970, pp. 93-95.

[5] Ardema, M. D., "Solution of the Minimum-Time-to-Climb Problem by Matched Asymptotic Expansions," *AIAA Journal*, Vol. 14, July 1976, pp. 843-850.

[6] Calise, A. J., "Extended Energy Management Methods for Flight Performance Optimization," *AIAA Journal*, Vol. 15, March 1977, pp. 314-321.

[7] Mehra, R., Washburn, R., Sajan, S., and Carrol, J., "A Study of the Application of Singular Perturbation Theory," NASA CR-3167, 1979.

[8] Calise, A. J., "A New Boundary Layer Matching Procedure for Singularly Perturbed Systems," *IEEE Transactions on Automatic Control*, Vol. AC-23, June 1978, pp. 434-438.